http://dx.doi.org/10.5012/bkcs.2011.32.11.3873

Isomerization and Dissociation of the Acrylonitrile Radical Cation: A Theoretical Study

Sun Hwa Jung, Gee-Hyung Lee, and Joong Chul Choe*

*Department of Chemistry, Dongguk University-Seoul, Seoul 100-715, Korea. *E-mail: jcchoe@dongguk.edu*
Received August 11, 2011, Accepted August 31, 2011

The potential energy surface (PES) for the isomerizations and dissociations of the acrylonitrile radical cation was determined from the CBS-QB3 and CBS-APNO calculations. The Rice-Ramsperger-Kassel-Marcus model calculations were performed based on the PES in order to predict the competitions among the dissociation channels. The mechanisms for the loss of $H^{\bullet}$, H_2, $CN^{\bullet}$, HCN, and HNC were proposed. The $C_3H_2N^+$ ion formed by loss of $H^{\bullet}$ was predicted as a mixture of CH≡C–C=NH^+, CH≡C–N≡CH^+, and CH_2=C–C≡N^+. Furthermore CH≡C–C≡$N^{+\bullet}$ was formed mainly by a consecutive 1,2-H shift and 1,2-H_2 elimination.

Key Words : Potential energy surface, CBS calculation, RRKM calculation, Kinetics, Reaction pathway

Introduction

Acrylonitrile (propenenitrile or vinyl cyanide) is one of the interstellar molecules detected spectroscopically.[1,2] The gas phase ion chemistry of acrylonitrile has been studied using several experimental and theoretical methods. The ion-molecule reactions related with acrylonitrile have been investigated by several groups.[3-9] For the characterization of the acrylonitrile ion, the following experimental techniques were used: electron attachment,[10] electron impact ionization,[11] charge exchange ionization,[12] and tandem mass spectrometry.[6-8,13]

The theoretical studies related with the acrylonitrile radical cation (CH_2=CH–C≡$N^{+\bullet}$, **A1**) were carried out by Terlouw and co-workers[6-8] and Takagi *et al*.[9] The theoretical association pathways of **A1** with HCN[6] and the theoretical isomerization pathways of the acrylonitrile dimer ion[8] were reported. To understand the ion-molecule reaction between the acetylene radical cation ($C_2H_2^{+\bullet}$) and HCN, the theoretical mechanisms for the loss of $H^{\bullet}$ and HCN from **A1**, which were two main dissociation channels in the metastable ion dissociation, were proposed.[7] It was suggested that CH≡C–C=NH^+ was formed by the loss of $H^{\bullet}$ and the ion-dipole complexes would be involved in the loss of HCN. Takagi *et al*.[9] suggested several pathways for the loss of $H^{\bullet}$ from some $C_3H_3N^{+\bullet}$ isomers that were formed by reacting $C_2H_2^{+\bullet}$ with HCN (or HNC).

A1 undergoes primary dissociations to four major fragment ions by the loss of $H^{\bullet}$, H_2, $CN^{\bullet}$, or HCN (or HNC). The relative abundances of the corresponding peaks in the 70-eV electron ionization mass spectrum[14] are 5.5, 2.2, 1.0, and 6.5, respectively, and those in the collision-induced dissociation (CID) spectrum[6] are 6.4, 2.6, 1.0, and 4.5, respectively. On the other hand, only the loss of $H^{\bullet}$ and HCN (or HNC) were detected in the metastable ion dissociation of **A1** with the relative abundance of 20:1.[7] In this work, a theoretical potential energy surface (PES) was examined for the isomerizations of **A1** and its primary dissociations to the four fragment ions. Various isomerization and dissociation pathways of **A1** were found. The dissociation kinetics is also discussed based on the PES.

Computational Methods

The molecular orbital calculations were performed with the CBS-QB3 and CBS-APNO model chemistry using the Gaussian 09 suite of programs.[15] In the CBS-QB3 and CBS-APNO methods, the energies are calculated with the geometries optimized at the B3LYP/6-311G(2d,d,p) and QCISD/6-311G(d,p) levels, respectively. Initially, the geometries of the minima were optimized at the unrestricted B3LYP level of the DFT using the 6-31G(d) basis set and at the unrestricted HF level using the 6-311G(d,p) basis set. The transition state (TS) geometries that connected the minima were examined and checked by calculating the intrinsic reaction coordinates at the same levels.

The RRKM expression was used to calculate the rate constant for the unimolecular reaction steps that were involved in the selected reaction pathways because the RRKM formula for the microcanonical ensemble was mathematically equivalent to the formula in the statistical quasi-equilibrium theory that was developed for ionic dissociations:[16]

$$k(E) = \frac{\sigma N^{\ddagger}(E-E_0)}{h\rho(E)} \quad (1)$$

In this equation, E is the internal energy of the reactant, E_0 is the critical energy of the reaction, $N^{\ddagger}$ is the sum of the TS states, ρ is the density of the reactant states, σ is the reaction path degeneracy, and h is Planck's constant. $N^{\ddagger}$ and ρ were evaluated through a direct count of the states using the Beyer-Swinehart algorithm.[17] Each normal mode of vibration was treated as a harmonic oscillator. The vibrational frequencies obtained from the B3LYP/6-311G(2d,d,p) calculations were scaled down by a factor of 0.969[18] and were then used for the RRKM calculation. The rate constants

were calculated at 0 K, which means that rotational effects were ignored.

Results and Discussion

Thermochemistry. The stable isomers of **A1** optimized in the CBS-QB3 calculations (actually at the B3LYP/6-311G(2d,d,p) level) are shown in Figure 1. The $C_3H_3N^{+\bullet}$ isomers are categorized into four groups; A, B, 3R, and 4R. Of which, A and B denote the linear CCCN and CCNC isomers, respectively, while 3R and 4R denote the three- and four-membered ring isomers, respectively. Their relative energies at 0 K and enthalpies of formation at 298 K were calculated using the QB3 and APNO methods, as shown in Table S1 (in Supplementary Materials), with those for the fragments. The relative energies and optimized structures obtained from the two methods showed a very good agreement except for **A7**. This is because a planar structure was optimized for **A7** in the APNO calculation, while the dihedral angle of HC1C2H (see Figure 1 for numbering) in **A7** optimized in the QB3 calculation was 80 degrees. Overall the calculated enthalpies of formation agreed with the experimental values for most of the species available in the literatures within approximately ± 10 kJ mol^{-1}.

Isomerization. The PES for the isomerizations of **A1**, derived from the CBS-QB3 calculations, is shown in Figure 2. The H on C2 shifts to C1 in order to form **A2**. The geometric structures optimized for the TSs during the isomerization are provided in Supplementary Materials. **A2** is a central intermediate for three further parallel isomerizations, forming **3R1**, **A3**, and **A7**. The ring closure to form a three-membered ring isomer **3R1** occurs easily by moving the N toward C2. Then, a skeleton rearrangement occurs by the C1–C2 bond cleavage to form CH_2=C=N=$CH^{+\bullet}$ (**B3**). This is the lowest energy pathway to form a B-type isomer starting from **A1**. The further isomerization of **B3** will be described later. The second isomerization from **A2** occurs by a further 1,2 shift of the H on C1 to the N, which forms the most stable isomer **A3**. The further isomerization from **A3** occurs by three consecutive 1,2 shifts of an H on C3 to C2, C1, and the N, which form (*E*)-**A4**, **A5**, and **A6**, respectively. (*E*)-**A4** easily isomerizes to (*Z*)-**A4**. A ring closure can occur from each of (*E*)- and (*Z*)-**A4** to form **3R2** and **4R1**, respectively. By the HC=CH bond cleavage of **4R1**, the ring is opened to form **B5**. **A5** forms **4R2** by a ring closure. Alternatively, **A3** can isomerize to **3R3** and further to **B2a** or **B2b**. The third isomerization from **A2** occurs by a 1,2 shift of an H on C3 to C2 to form **A7**. **A7** easily isomerizes to (*Z*)-**B4** by a rotation of the HCN moiety or to **4R3** by a ring closure. (*Z*)-**A4** can again isomerize to **A7** or **B7**. The H on C2 of **A1** can shift to C3 to form **A8**, which acts as an intermediate in the loss of H_2 as described later.

The isocyanoethylene radical cation (CH_2=CH–N≡$C^{+\bullet}$, **B1**) is formed from **A1** by the rotation of the CN moiety. Interestingly, the formation of the other B-type isomers from **B1** is approximately parallel with that of the corresponding A-type isomers from **A1**. **B2a** formed by a 1,2 shift of the H on C2 to the N is also a central intermediate in the further isomerization to B-type isomers. Similarly with the isomerization of **A2**, **B2a** can undergo three parallel pathways; **B2a**

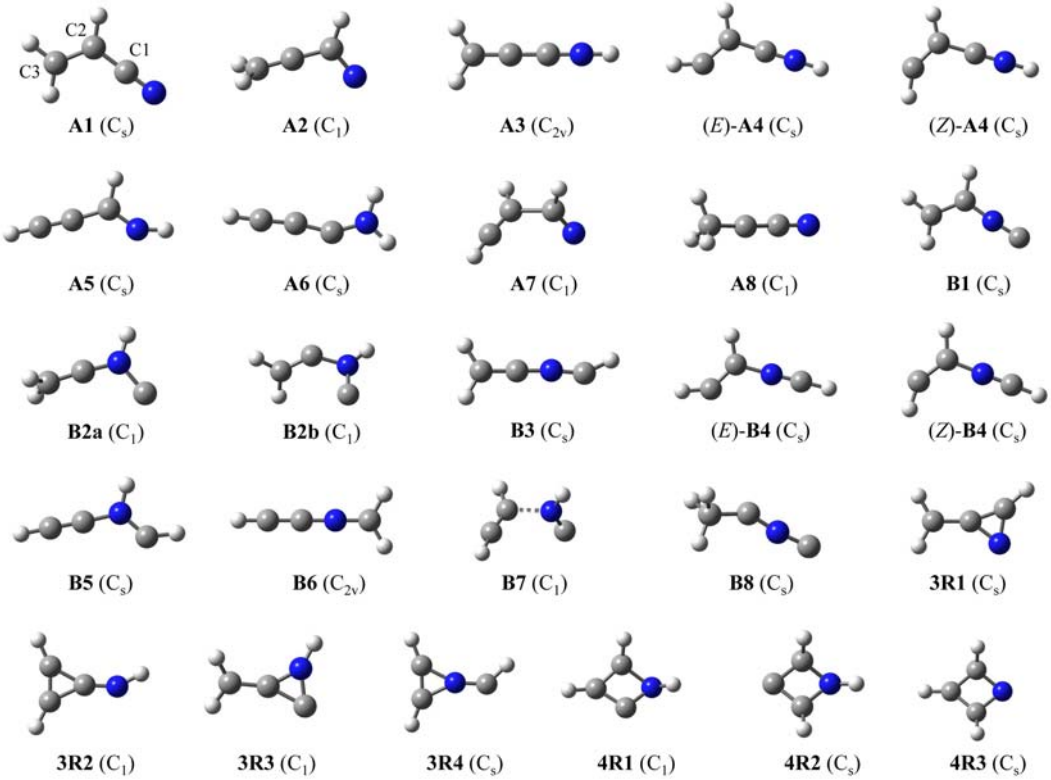

Figure 1. Geometric structures for $C_3H_3N^{+\bullet}$ isomers optimized using the CBS-QB3 calculations.

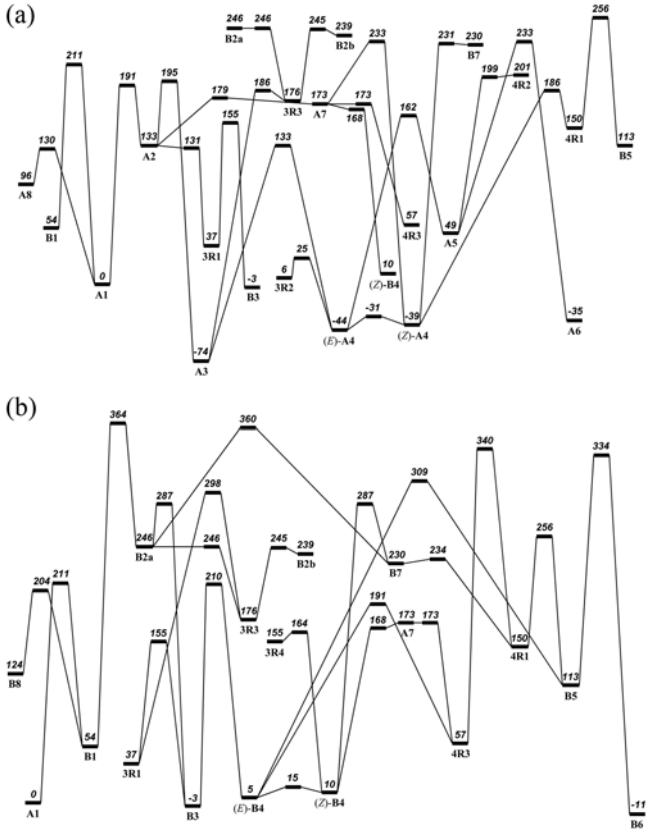

Figure 2. Potential energy diagram for the isomerizations of **A1** occurring (a) mainly *via* **A2** and (b) *via* **B1**, which was derived from the CBS-QB3 calculations. The energies are in kJ mol^{-1}.

→ **3R3** → **A3**, **B2a** → **B3** → (*E*)-**B4**, and **B2a** → **B7** → **4R1**. The pathways from **B4** to form the isomers **4R3**, **B5**, **B6**, **A7**, **3R4**, and **B7** are similar to the further isomerization of **A4**; though a major difference distinguishes them is that the two structures were optimized for **B2**. **B2a** and **B2b** are easily convertible. The optimized angles of C3C2N in **B2a** and **B2b** were 176 and 135 degrees, respectively. In contrast, the corresponding more bent isomer of **A2** was not optimized. **B8** can be formed from **B1** by a 1,2-H shift. However, the pathways shown in Figure 2(b) were not the lowest energy pathways for some B-type isomers. The formation of **B2**, **B3**, **B4**, or **B7** occurring through **A2**, shown in Figure 2(a), is energetically more favored than that through **B1** as indicated in Figure 2(b).

Dissociation. The following dissociation reactions were examined in this work.

$$CH_2{=}CH{-}C{\equiv}N^{+\bullet} \rightarrow CH{\equiv}C{-}C{=}NH^{+} + H^{\bullet} \quad (2)$$
$$CH_2{=}CH{-}C{\equiv}N^{+\bullet} \rightarrow CH{\equiv}C{-}N{\equiv}CH^{+} + H^{\bullet} \quad (3)$$
$$CH_2{=}CH{-}C{\equiv}N^{+\bullet} \rightarrow CH_2{=}C{-}C{\equiv}N^{+} + H^{\bullet} \quad (4)$$
$$CH_2{=}CH{-}C{\equiv}N^{+\bullet} \rightarrow CH{\equiv}C{-}C{\equiv}N^{+\bullet} + H_2 \quad (5)$$
$$CH_2{=}CH{-}C{\equiv}N^{+\bullet} \rightarrow C_2H_3^{+} + CN^{\bullet} \quad (6)$$
$$CH_2{=}CH{-}C{\equiv}N^{+\bullet} \rightarrow C_2H_2^{+\bullet} + HCN \quad (7)$$
$$CH_2{=}CH{-}C{\equiv}N^{+\bullet} \rightarrow C_2H_2^{+\bullet} + HNC \quad (8)$$

Loss of H$^{\bullet}$: First of all, possible 15 $C_3H_2N^+$ isomers were optimized to find the reasonable pathways for the loss of H$^{\bullet}$ from **A1**. Their obtained geometric structures and energies are available in Supplementary Materials. The N-protonated cyanoacetylene cation (CH≡C–C=NH$^+$) was the most stable, which is well known.[19] The next were the protonated isocyanoacetylene cation (CH≡C–N≡CH$^+$) and the C-protonated cyanoacetylene cation (CH$_2$=C–C≡N$^+$), which were less stable by 77 and 162 kJ mol^{-1} relative to CH≡C–C=NH$^+$, respectively. Unless otherwise stated, the energies presented in this text refer to the total energies at 0 K derived from the CBS-QB3 calculations. The pathways for the formation of these three $C_3H_2N^+$ isomers, reactions 2-4, were obtained.

Considering only the exit channel, the formation of CH≡C–C=NH$^+$ is possible by a direct C–H bond cleavage from **A3**, **A4**, or **A5** or by a direct N–H bond cleavage from **A6**. Among these possibilities the elimination of H$^{\bullet}$ from **A3** is kinetically the most probable pathway when dissociating from **A1**. This is because **A4**, **A5**, and **A6** are formed by the further consecutive isomerization of **A3**. According to the RRKM rate constant calculations, the isomerization **A3** → (*E*)-**A4**, followed by the dissociation, was less favored by a factor of 2-4, dependant on the internal energy, than the dissociation **A3** → HC≡C–C=NH$^+$ + H$^{\bullet}$. The formation of HC≡C–C=NH$^+$ *via* **A5** and **A6** is negligible because the formation of these intermediates was much less favored energetically than that of **A3** or **A4**. The TS for the elimination of H$^{\bullet}$ from **A3** was found (Figure 3). The PES for the dissociations is shown in Figure 4.

Similarly, the formation of CH≡C–N≡CH$^+$ is possible by a direct C–H or N–H bond cleavage from **B3-B6** considering only the exit channel. However, only the loss of H$^{\bullet}$ *via* **B3** or **B4** was important because the barriers needed to form **B2**, **B5**, and **B6** from **A1** were much higher than those required to form **B3** and **B4**. The TS for the elimination of H$^{\bullet}$ from **B3** lies lower than the TS for that from (*E*)-**B4** (Figure 4(a)).

The direct elimination of H$^{\bullet}$ from **A1** is possible from C2 or C3, which produces CH$_2$=C–C≡N$^+$ or CH=CH–C≡N$^+$, respectively. The formation of the latter cation is much less favored than that of the former because the calculated energy of the latter was 57 kJ mol^{-1} higher than that of the former. The TS for the dissociation to CH$_2$=C–C≡N$^+$ + H$^{\bullet}$ was found (Figure 3). Alternatively, CH$_2$=C–C≡N$^+$ can be formed from an elimination of H$^{\bullet}$ from **A8**.

Loss of H$_2$: Among possible $C_3HN^{+\bullet}$ isomers that can be formed by the loss of H$_2$, only the propiolonitrile radical cation (CH≡C–C≡N$^{+\bullet}$) and isocyanoacetylene radical cation (CH≡C–N≡C$^{+\bullet}$) have been observed in the experiment.[19] The former or latter radical cations can be produced by a 1,2-H$_2$ elimination from **A1** or **B1**, respectively. The previous G2 calculation[20] showed that the former is more stable than the latter by 72 kJ mol^{-1}, which implies that the formation of the latter is much less favored. Therefore, only the "apparent" 1,2-H$_2$ elimination from **A1** to form CH≡C–C≡N$^{+\bullet}$ was examined in this work. The elimination of H$_2$ from small gas phase ions has been well reviewed by Uggerud.[21] After the formation of **A8**, two H atoms on C3 depart to form an ion-dipole complex, **ID1**, and then H$_2$ is eliminated to produce CH≡C–C≡N$^{+\bullet}$ (path I_{-H_2}). Considering only the latter two steps, this is a 1,1-elimination,

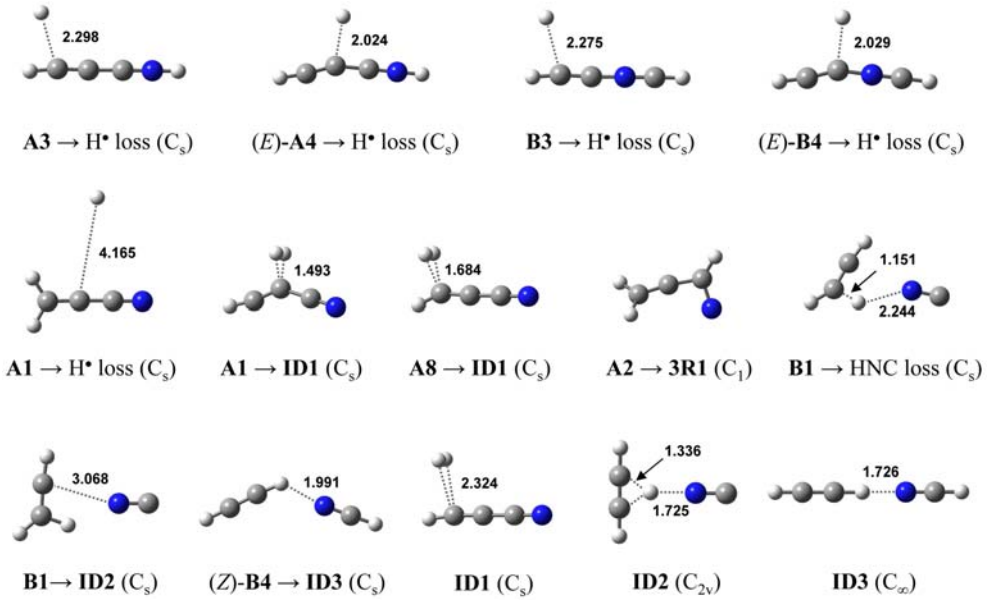

Figure 3. Geometric structures for selected transition states and the ion-dipole complexes optimized using the CBS-QB3 calculations. Those for **ID2** and TS **B1** → **ID2** were the results of the CBS-APNO and B3LYP/6-311G(d) calculations, respectively. The distances are in Å.

whereas the whole reaction starting from **A1** can be a 1,2 or 1,1-elimination relying on whether the shifted H atom from C2 can be eliminated or not. Alternatively, an H atom on C3 of **A1** shifts to C2 and then is eliminated together with the H on C2 (path II_{-H_2}). This is therefore a 1,2-elimination. The structures of TS **A8** → **ID1** and the TS in path II_{-H_2} are similar except that the position of the departing H_2 moiety (see Figure 3). The lengths of H–H and C–H of the former are 0.797 and 1.684 Å, respectively, and those of the latter are 0.833 and 1.493 Å, respectively. The main difference between path I_{-H_2} and path II_{-H_2} is a stable isomer, **A8**, is formed after the H-shift in the former, while any stable intermediate is not formed in the latter. The barrier for path I_{-H_2} is 50 kJ mol^{-1} lower than that for path II_{-H_2}.

Loss of CN•, HCN, and HNC: It is well known that the non-classical proton bridged acetylene is the best structure of $C_2H_3^+$, which is formed by the loss of CN• from **A1**. After the isomerization to **B1**, the CN moiety leaves C2 to form an ion-dipole complex, **ID2**, according to B3LYP/6-31G(d) and B3LYP/6-311G(d) calculations. The elimination of CN• from **ID2** forms the proton bridged acetylene. The TS was located at 87 kJ mol^{-1} lower than $C_2H_3^+$ + CN• according to the B3LYP/6-311G(d) calculation. However, the TS could not be optimized in the QB3 and APNO calculations.

The loss of HCN can occur directly from **A7** or *via* (*Z*)-**B4**. The HCN moiety of (*Z*)-**B4** goes away from C2 to form an ion-dipole complex, **ID3**. Then, $C_2H_2^{+\bullet}$ is formed by the elimination of HCN. It was mentioned that any ion-dipole complex $[HCN\cdots C_2H_2]^{+\bullet}$ was not optimized as a stable species in the report by Terlouw and co-workers.[7] The loss of HNC thus can occur *via* **B1**. As the CN moiety of **B1** goes away from C2, the H on C3 moves toward the N to form $C_2H_2^{+\bullet}$ + HNC. Alternatively, HNC can be eliminated directly from **A4**. However, the loss of HNC is less favored than the loss of HCN because HNC is less stable than the HCN by 59 kJ mol^{-1}.

Kinetics: To obtain an insight into the dissociation kinetics, the rate constants of some reaction steps were calculated using the RRKM formula (Equation 1) by assuming that the dissociation occurred statistically on the ground electronic state. The critical energies calculated from the CBS-QB3 energy data were used in the RRKM calculation.

Figure 5 shows the energy dependence of the RRKM rate constants, $k(E)$s, for the reactions occurring from **A1**; **A1** → CH_2=C–C≡N$^+$ + H•, **A1** → **A8** → **ID1** → CH≡C–C≡N$^{+\bullet}$ + H_2, **A1** → **A2**, and **A1** → **B1**. The $k(E)$ for the formation of CH_2=C–C≡N$^+$ + H• *via* **A8** was smaller than that for the formation by the direct C–H bond cleavage from **A1**, shown in Figure 5, by about one order of magnitude. This is because TS **A8** → CH_2=C–C≡N$^+$ + H• lies higher than the TS **A1** → CH_2=C–C≡N$^+$ + H•. In the rate constant calculation for **A1** → **A8** → **ID1** → CH≡C–C≡N$^{+\bullet}$ + H_2 (path I_{-H_2}), shown in Figure 5, it was assumed that the dissociation occurred in one step through TS **A8** → **ID1** from **A1** because the other steps hardly affected the dissociation rate. The $k(E)$ for path II_{-H_2} was smaller than that for path I_{-H_2} by 4-1 orders of magnitude at the internal energies of 310-600 kJ mol^{-1}.

Comparing the rate constants for the formation of CH_2=C–C≡N$^+$ + H• and CH≡C–C≡N$^{+\bullet}$ + H_2, shown in Figure 5, the former is favored at high energies, while the latter is favored at low energies. At energies higher than about 400 kJ mol^{-1}, these dissociations occur faster than the isomerization to **A2** or **B1**, which indicates that at high energies the formation of CH_2=C–C≡N$^+$ + H• is much favored over the loss of H_2 that is also a competitive path. On comparison, at low energies, the rate constant of **A1** → **A2** is the largest as shown in Figure 5, which implies other dissociation channels might be of crucial importance as well. This is so because **A2** is the first and common intermediate in reactions 3, 4, 6, 7, and 8.

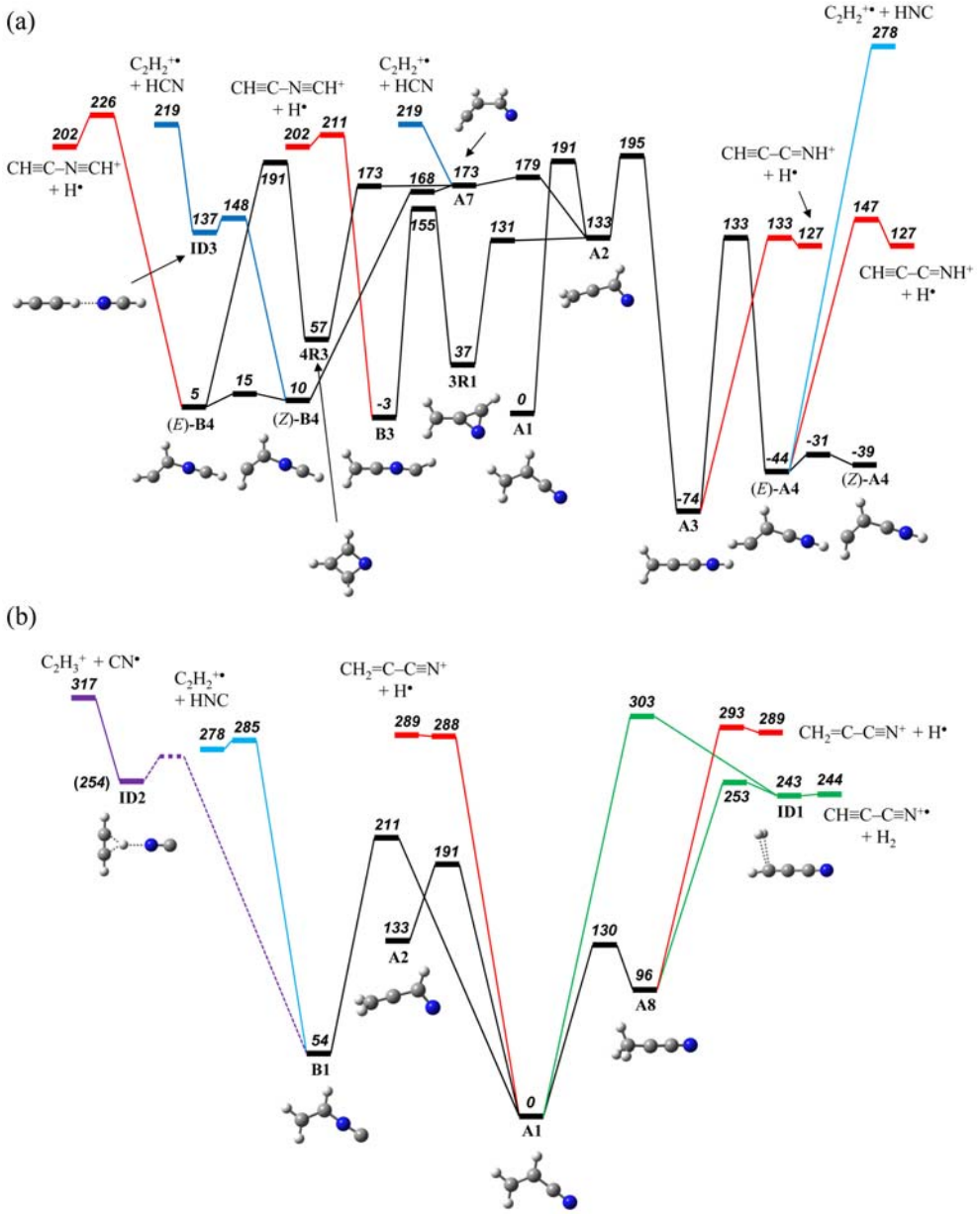

Figure 4. Potential energy diagram for the dissociations of **A1** occurring (a) *via* **A2** and (b) not *via* **A2**, which was derived from the CBS-QB3 calculations. The energies are in kJ mol^{-1}. The energy of **ID2** is calculated from the CBS-APNO method.

Figure 6 shows the RRKM rate constants for the isomerization of **A2**. Once **A2** is formed, it undergoes rapid further isomerization rather than the reverse isomerization. Interestingly, the slope of the $k(E)$ for the isomerization **A2** → **3R1**, which eventually dissociate to CH≡C–N≡CH$^+$ + H$^\bullet$, is much smaller than the others. This is because the corresponding TS is very tight. The entropy of activation[16,22] at 1000 K of the isomerization **A2** → **3R1** was 29 J mol^{-1} K^{-1}. The rate constant at 200 kJ mol^{-1} was very large due to the nearly zero critical energy but hardly increased with the ion internal energy. It should be noted that the negative critical energy (−2 kJ mol^{-1}) for the isomerization **A2** → **3R1** is not realistic. This is probably because the CBS-QB3 method is a compound method, not based on a single-level calculation. For example, the critical energy calculated at the B3LYP/6-311G(2d,d,p) level was 3 kJ mol^{-1}, which was used for the rate constant calculation shown in Figure 6.[23] The $k(E)$s shown in Figure 6 indicate that at low energies the isomerization to **3R1** is dominant but as the energy increases the isomerizations to **A7** and **A3** become more important. **A7** is the intermediate to form CH≡C–N≡CH$^+$ + H$^\bullet$ and $C_2H_2^{+\bullet}$ + HCN, and **A3** is the intermediate to form CH≡C–C=NH$^+$ + H$^\bullet$. However, their branching ratios cannot be determined solely from the competitive isomerization of **A2**. In the formation of CH≡C–C=NH$^+$ + H$^\bullet$, the isomerization **A2** → **A3** is the rate-limiting step, but the other dissociation channels occurring *via* **A2** have the highest barriers at the final dissociation steps. At the internal energies of 195-211 kJ mol^{-1}, only the formation of CH≡C–C=NH$^+$ + H$^\bullet$ *via* **A3** (reaction 2) is possible. However, as the energy increases,

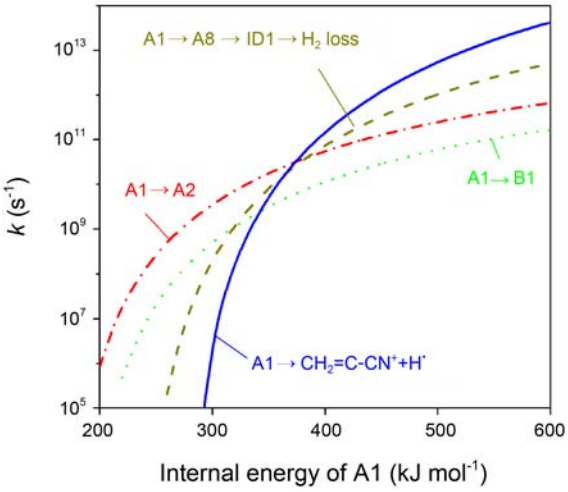

Figure 5. Energy dependence of the RRKM rate constants for the reactions **A1** → CH_2=C–C≡N^+ + H$^\bullet$, **A1** → **A8** → **ID1** → CH≡C–C≡$N^{+\bullet}$ + H_2, **A1** → **A2**, and **A1** → **B1**.

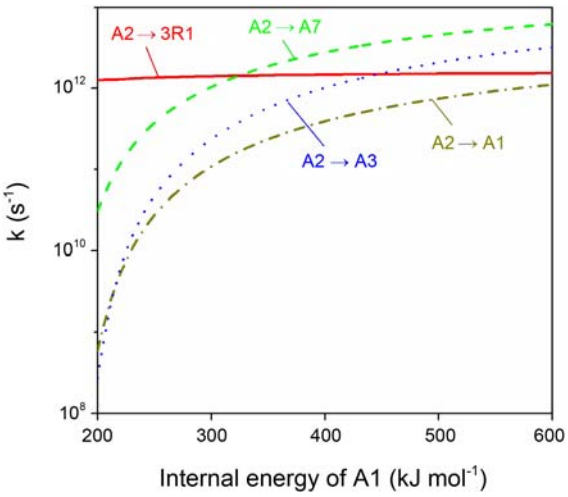

Figure 6. Energy dependence of the RRKM rate constants for the isomerizations of **A2** to **A1**, **A3**, **A7**, and **3R1**.

the formation of CH≡C–N≡CH^+ + H$^\bullet$, $C_2H_2^{+\bullet}$ + HCN, and CH≡C–N≡CH^+ + H$^\bullet$, where the first one occurs *via* **3R1** and the rests are *via* **A7**, start to play an important part. Therefore, this predicts CH≡C–C=NH^+ as the main product in the metastable ion dissociation in which $C_3H_2N^+$ and $C_2H_2^{+\bullet}$ (20:1) were detected.[7] In addition, the detection of $C_2H_2^{+\bullet}$ in the metastable ion dissociation is the result of the loss of HCN, and the formation of CH≡C–N≡CH^+ would contribute to the loss of H$^\bullet$ because it competes with the loss of HCN.

The loss of CN$^\bullet$ was detected in the mass and CID spectra even though its relative abundance was small. The endoergicity (317 kJ mol^{-1}) of reaction 6, higher than those of the other dissociation channels, makes the loss of CN$^\bullet$ least favorable. Because the endoergicity (278 kJ mol^{-1}) of reaction 8 is lower than that of reaction 6, the loss of HNC would contribute to the formation of $C_2H_2^{+\bullet}$, even though it is less favored.

Comparison with the Experimental Data: As described in the Introduction section, the relative product abundances in the reported mass[14] and CID[6] spectra are similar. The loss of H$^\bullet$ and HCN are the two major dissociation channels. According to the present prediction, the loss of H$^\bullet$ is the most favorable channel both energetically and kinetically. The high abundance of the loss of HCN in the mass and CID spectra could not be well interpreted only with the present kinetic analysis. It should be noted that fragment ions detected in mass and CID spectra are the results of several competitive and consecutive reactions because the molecular ions generated possess relatively high energies with a broad distribution. In contrast, the metastable ions possess relatively low energies corresponding to the lifetimes of microseconds. The fact that the only major fragment ion in the metastable ion dissociation[7] is $C_3H_2N^+$ agrees well with the present result. The further experimental studies are needed with the energy-defined ions to understand the kinetics more deeply.

Conclusions

The isomerization pathways of **A1** were determined theoretically. Among the optimized $C_3H_3N^{+\bullet}$ isomers, **A3** (CH_2=C=C=$NH^{+\bullet}$) was the most stable. **A2** (CH_2=C–CH=$N^{+\bullet}$) formed by the 1,2-H shift was the most important intermediate in the isomerization and dissociation of **A1**. The mechanisms for the main dissociation channels detected in the metastable ion dissociation and the CID were determined. Three isomeric $C_3H_2N^+$ ions were formed by the loss of H$^\bullet$. It was predicted that the formation of CH≡C–C=NH^+ and CH≡C–N≡CH^+ were favored at low energies, whereas the formation of CH_2=C–C≡N^+ was favored at high energies according to the RRKM calculations. For the loss of H_2, the formation of CH≡C–C≡$N^{+\bullet}$ occurred more favorably by the consecutive 1,2-H shift and 1,2-H_2 elimination than by the one-step 1,2-H_2 elimination. The formation of $C_2H_2^{+\bullet}$ could occur by the elimination of HCN, before or after the CCCN skeleton arrangement, from **A7** (CH=CH–CH=$N^{+\bullet}$) and **B4** (CH=CH–N≡$CH^{+\bullet}$), respectively. The isomerization to **B1** (CH_2=CH–N≡$C^{+\bullet}$) was the first step in the loss of CN$^\bullet$ and HNC.

Acknowledgments. This work was supported by a National Research Foundation of Korea Grant funded by the Korean Government (2011-0005028).

Supplementary Materials. Calculated thermochemical data for the $C_3H_3N^{+\bullet}$ isomers and the fragments and geometric structures for the transition states connecting the $C_3H_3N^{+\bullet}$ isomers and the $C_3H_2N^+$ isomers optimized using the CBS-QB3 calculations.

References

1. Gardner, F. F.; Winnewisser, G. *Astrophys. J.* **1975**, *195*, L127.
2. Snyder, L. E. *Proc. Natl. Acad. Sci.* **2006**, *103*, 12243.

3. Petrie, S.; Chirnside, T. J.; Freeman, C. G.; McEwan, M. J. *Int. J. Mass Spectrom. Ion Processes* **1991**, *107*, 319.
4. Petrie, S.; Freeman, C. G.; McEwan, M. J. *Mon. Not. R. Astr. Soc.* **1992**, *257*, 438.
5. Sun, J.; Grützmacher, H. F.; Lifshitz, C. *J. Am. Chem. Soc.* **1993**, *115*, 8382.
6. Ervasti, H. K.; Jobst, K. J.; Gerbaux, P.; Burgers, P. C.; Ruttink, P. J. A.; Terlouw, J. K. *Chem. Phys. Let.* **2009**, *482*, 211.
7. Jobst, K. J.; Hasan, S. A.; Terlouw, J. K. *Chem. Phys. Let.* **2008**, *450*, 243.
8. Ervasti, H. K.; Jobst, K. J.; Burgers, P. C.; Ruttink, P. J. A.; Terlouw, J. K. *Int. J. Mass Spectrom.* **2007**, *262*, 88.
9. Takagi, N.; Fukuzawa, K.; Osamura, Y.; Schaefer III, H. F. *Astrophys. J* **1999**, *525*, 791.
10. Heni, M.; Illenberger, E. *Int. J. Mass Spectrom. Ion Processes* **1986**, *73*, 127.
11. Gluch, K.; Cytawa, J.; Michalak, L. *Int. J. Mass Spectrom.* **2008**, *278*, 10.
12. Youn, Y. Y.; Choe, J. C.; Kim, M. S. *Am. Soc. Mass Spectrom.* **2003**, *14*, 110.
13. Ichihashi, M.; Tsukuda, T.; Nonose, S.; Kondow, T. *J. Phys. Chem.* **1995**, *99*, 17354.
14. *NIST Chemistry WebBook, NIST Standard Reference Database Number 69*.
15. Frisch, M. J. T., G. W.; Schlegel, H. B.; Scuseria, G. E.; Robb, M. A.; Cheeseman, J. R.; Scalmani, G.; Barone, V.; Mennucci, B.; Petersson, G. A.; Nakatsuji, H.; Caricato, M.; Li, X.; Hratchian, H. P.; Izmaylov, A. F.; Bloino, J.; Zheng, G.; Sonnenberg, J. L.; Hada, M.; Ehara, M.; Toyota, K.; Fukuda, R.; Hasegawa, J.; Ishida, M.; Nakajima, T.; Honda, Y.; Kitao, O.; Nakai, H.; Vreven, T.; Montgomery, J. A., Jr.; Peralta, J. E.; Ogliaro, F.; Bearpark, M.; Heyd, J. J.; Brothers, E.; Kudin, K. N.; Staroverov, V. N.; Kobayashi, R.; Normand, J.; Raghavachari, K.; Rendell, A.; Burant, J. C.; Iyengar, S. S.; Tomasi, J.; Cossi, M.; Rega, N.; Millam, N. J.; Klene, M.; Knox, J. E.; Cross, J. B.; Bakken, V.; Adamo, C.; Jaramillo, J.; Gomperts, R.; Stratmann, R. E.; Yazyev, O.; Austin, A. J.; Cammi, R.; Pomelli, C.; Ochterski, J. W.; Martin, R. L.; Morokuma, K.; Zakrzewski, V. G.; Voth, G. A.; Salvador, P.; Dannenberg, J. J.; Dapprich, S.; Daniels, A. D.; Farkas, Ö.; Foresman, J. B.; Ortiz, J. V.; Cioslowski, J.; Fox, D. J. *Gaussian 09, revision A. 02*; Gaussian, Inc., Wallingford CT, 2009.
16. Baer, T.; Hase, W. L. *Unimolecular Reaction Dynamics: Theory and Experiments*; Oxford University Press: New York, 1996.
17. Beyer, T.; Swinehart, D. R. *ACM Commun.* **1973**, *16*, 379.
18. The scaling factor for the B3LYP/6-311G(2d,d,p) calculation has not been reported. Because the scaling factor reported for the B3LYP/6-311+G(2d,p) calculation is 0.9692, we used 0.969 for the B3LYP/6-311G(2d,d,p) calculation.
19. Holmes, J. L.; Aubry, C.; Mayer, P. M. *Assigning Structures to Ions in Mass Spectrometry*; CRC Press: Boca Raton, 2007.
20. Barrientos, C.; Redondo, P.; Largo, A. *J. Phys. Chem. A* **2000**, *104*, 11541.
21. Uggerud, E. *Mass Spectrom. Rev.* **1999**, *18*, 285.
22. The entropy of activation is usually used as a quantitative measure of the degree of "tightness" of the transition state. It is higher or lower than the zero for a loose or tight transition state, respectively.
23. The use of the critical energies in the range of 2 to 3 kJ mol^{-1} did not affect the $k(E)$ largely. The rate constants calculated using E_0 = 2 kJ mol^{-1} were less than those using E_0 = 3 kJ mol^{-1} by a factor of 0.6 and 0.9 at the ion internal energy of 200 and 600 kJ mol^{-1}, respectively.